Performance Analysis of a Utility Helicopter with Standard and Advanced Rotors

Hyeonsoo Yeo
Raytheon ITSS

William G. Bousman
Army/NASA Rotorcraft Division
Aeroflightdynamics Directorate (AMRDEC)
US Army Aviation and Missile Command

Wayne Johnson
Army/NASA Rotorcraft Division

NASA Ames Research Center
Moffett Field, California

Abstract

Flight test measurements of the performance of the UH-60 Black Hawk helicopter with both standard and advanced rotors are compared with calculations obtained using the comprehensive helicopter analysis CAMRAD II. In general, the calculated power coefficient shows good agreement with the flight test data. However, the accuracy of the calculation degrades at high gross weight for all of the configurations. The analysis shows fair to good correlation for collective and longitudinal cyclic angles and pitch attitude, and poor to fair correlation for the lateral trim quantities (lateral cyclic angle and roll attitude). The increased solidity of the wide chord blade appears to be a dominant factor in the performance improvement at high gross weight by reducing blade loading and thus delaying stall.

Notation

C_p	power coefficient
C_w	weight coefficient
D	fuselage drag
M	Mach number
q	dynamic pressure
α	angle of attack
α_s	aircraft pitch attitude
μ	advance ratio
σ	solidity

Introduction

The ability to accurately predict the performance of a helicopter is essential for the design of future rotorcraft. Before prediction codes can be successfully used, it is necessary to assess their accuracy and reliability. Comparison of comprehensive analysis performance calculations with helicopter flight test data is crucial to such an assessment.

With the completion of recent flight tests, performance and dynamic data are available for the standard UH-60 blades tested on a UH-60A airframe [1]; the standard blades on a UH-60L airframe [2]; and several different versions of the wide chord blades on the same UH-60L airframe [2]. These extensive flight test data sets provide a valuable bench mark for the evaluation of comprehensive methods. In this study, performance calculations were carried out using the analysis CAMRAD II and the results are compared with these UH-60 flight test data.

Flight Test Data

Test data with the UH-60A standard (STD) blades were obtained on a UH-60A airframe in the NASA/Army UH-60A Airloads Program conducted from August 1993 to February 1994 [1]. The test aircraft, 82-23748, is a sixth-year production aircraft. The data obtained from the test are stored in an electronic data base at NASA Ames Research Center. The standard blade is constructed using a titanium spar with a fiberglass outer contour. The blade uses two airfoils, the SC1095 and SC1094 R8. This blade has been used on the Black Hawk over the last 25 years.

The wide chord blade (WCB) is a development blade which has an all composite graphite/glass tubular spar. The wide chord blade incorporates an increased chord (10% increase of solidity), advanced airfoils (SC2110 and SSCA09), and a swept-tapered tip with anhedral. Six configurations or variants of the wide chord blade have been tested: configurations 1, 2, 3, 4, 4A, and 5. The differences between these configurations are mostly in the mid-span and leading edge tip weights. All the results shown here are for configuration 4A. The standard and wide chord blade planforms are shown in Figure 1. The wide chord blade data used here were obtained from a joint Sikorsky/Army feasibility flight

Presented at the American Helicopter Society Aerodynamics, Acoustics, and Test and Evaluation Technical Specialist Meeting, San Francisco, CA, January 23-25, 2002.

test program conducted from November 1993 through October 1995 (Appendix B of Ref. 2). The wide chord blades were tested on an aircraft 84-23953, which is a UH-60A upgraded to a UH-60L for test purposes.

CAMRAD II Modeling

The UH-60 Black Hawk was modeled in CAMRAD II [3] as an aircraft with single main and tail rotors. The current model has been updated from a previous UH-60A study [4] using CAMRAD II. The UH-60A master input database is available to qualified researchers. Minor changes have been made in chord length, quarter chord location, c.g. offset, pitch link geometry and the detailed representation of material properties. The SC1095 and SC1094 R8 airfoil decks are same as used in Ref. 4.

The wide chord blade structural and aerodynamic properties were obtained from Ref. 5. Section lift, drag, and moment values for the SC2110 and SSCA09 airfoils were obtained from airfoil C81 decks developed by Sikorsky Aircraft.

The trim solution used in CAMRAD II is based on the aircraft gross weight, c.g., flight speed, rotor rpm, density, and outside air temperature and solves for the controls and aircraft attitudes that balance the forces and moments with zero sideslip angle. For the standard blade on the UH-60A aircraft, the horizontal stabilator angle was set to match the measured flight test values from the UH-60A Airloads Program. No equivalent measurement was available for the UH-60L test data so the stabilator angle was set based on Airloads Program measurements at given C_w and μ values. An aerodynamic interference model in CAMRAD II was used for the performance calculations. This includes the main rotor inflow interference effects on wing-body and tail and the tail rotor, as time-averaged wake-induced velocity changes. No empirical factor was used for the calculation of the interference.

The aerodynamic characteristics of the UH-60 fuselage are based on 1/4th scale wind tunnel tests reported in Ref. 6. Only fuselage drag value was updated to accommodate configuration changes.

Fuselage Drag Configuration

The baseline UH-60A fuselage drag equations from the wind tunnel test [6] are:

$$D/q\ (\text{ft}^2) = 19.0 + 0.0095\,(1.66\,\alpha_s)^2 \quad \text{Tail off}$$
$$D/q\ (\text{ft}^2) = 22.0 + 0.0160\,(1.66\,\alpha_s)^2 \quad \text{Tail on}$$

where q is dynamic pressure and α_s is pitch attitude in degrees. The tail off configuration includes only the basic fuselage and the tail on configuration includes the stabilator, vertical tail, and tail rotor head as well. The zero angle of attack drag value depends upon the aircraft configuration and tends to increase as new modifications are made to the aircraft. However, it is assumed that the measured variation of drag with angle of attack is not affected by these aircraft configuration changes.

There are four possibilities for the equivalent flat plate area of the Airloads Program aircraft and these are summarized in Table 1. These four cases differ depending upon both baseline drag and the drag of aircraft modifications. There are two baseline values for a zero angle of attack drag. One is Sikorsky's value, 25.69 ft^2 from their flight manual performance substantiating report [7], which is the basic reference for the aircraft's handbook performance. The other value, 26.2 ft^2, is from the study by Shanley [12], which was performed under a NASA contract.

The aircraft as tested in the Airloads Program differs from the baseline in two respects. First, the aircraft is a sixth-year production version and therefore includes the External Stores Support System (ESSS) fairings and miscellaneous changes such as a deice system distributor assembly and an ice detector probe. In addition, a wire strike kit has been added to this aircraft to upgrade it to fleet standard. Sikorsky [7] has computed the effects of these modifications differently than the US Army Aviation Engineering Flight Activity (AEFA) [9–11]. Sikorsky's estimate of the equivalent flat plate area of ESSS fairings, miscellaneous, and wire strike kit was 0.78 ft^2, 0.63 ft^2, and 0.21 ft^2 respectively. AEFA's estimate for those components was 2.5 ft^2 [9], 1.0 ft^2 [10], 1.0 ft^2 [11]. Second, specific instrumentation was added to the aircraft for the test program. The drag for the Blade Motion Hardware (BMH), Low AirSpeed Sensing and Indicating Equipment (LASSIE), and test instrumentation was determined by AEFA. The drag of the Rotating Data Acquisition System (RDAS) was based on its projected area.

The equivalent flat plate area of the Airloads Program aircraft was calculated based on the following equation:

Airloads Program A/C = Baseline UH-60A (1st year A/C) + ESSS fairing + wire strike kit + misc.
+ BMH/LASSIE + test instrumentation + RDAS

The four possible cases shown in Table 1 are: (1) Case 1 : Sikorsky's baseline drag + Sikorsky's drag build-up, (2) Case 2 : Shanley's baseline drag + Sikorsky's drag build-up, (3) Case 3 : Sikorsky's baseline drag + AEFA's drag build-up, and (4) Case 4 : Shanley's baseline drag + AEFA's drag build-up. The final flat plate area, then, varies from 32.95 ft^2 to 36.34 ft^2. The current analysis

uses a zero angle of attack drag value of 35.14 ft^2 for the UH-60A, which is very close to the Case 3 value. For the UH-60L, a flat plate area of 35.04 ft^2 was used, as this provided the best match of parasite drag at high speed. This value is about 10% higher than the value specified by Sikorsky [2] for this configuration. The fuselage drag equations used in the present calculations are:

$$D/q\ (\text{ft}^2) = 35.14 + 0.016\,(1.66\,\alpha_s)^2$$
for UH-60A (Airloads Program)

$$D/q\ (\text{ft}^2) = 35.04 + 0.016\,(1.66\,\alpha_s)^2$$
for UH-60L

Results and Discussion

UH-60A Performance

The total power coefficient for the UH-60A was calculated using CAMRAD II and is compared with level flight data obtained in the Airloads Program for six weight coefficients in Figure 2. The total power coefficient is the sum of each engine's power, based on an engine output shaft torque sensor and the output shaft speed. The trim solution used in CAMRAD II solves for the controls and aircraft attitudes that balance the forces and moments in flight with zero sideslip angle. Performance was calculated using nonuniform inflow with a free wake geometry and a zero angle of attack drag value of 35.14 ft^2. CAMRAD II calculates only the main rotor and tail rotor power. Thus the fixed accessory power of 65.8 HP [7] was added to the CAMRAD II calculations.

In general, the estimated power coefficient shows good agreement with the flight test data. At low speeds ($\mu \leq 0.1$), the analysis tends to underpredict the power coefficient. The reasons are threefold: (1) airspeed measurements degrade at lower airspeeds as the dynamic pressure is reduced, (2) trim conditions are more difficult to maintain, and (3) computed power is strongly influenced by induced power which is more sensitive to wake effects. This correlation will be discussed quantitatively in the section "Quantitative Performance Correlation." As weight coefficient increases, larger differences are seen between the calculations and measurements.

The calculated main rotor power coefficient is compared with the measured value in Figure 3. This is the same calculation as in Figure 2, except that only main rotor power is compared. Main rotor power coefficient data for the UH-60A were calculated based on the measurement of the main rotor torque. The analysis shows good agreement with the flight test data. Slightly better correlation is observed than with the total engine power.

Figure 4 compares the calculated tail rotor power with the test data. Tail rotor power coefficient data were calculated based on the measurement of the intermediate shaft torque. The analysis underpredicts at low speeds and overpredicts at moderate speeds up to C_w of 0.0091. However, an overprediction is observed at all speeds at C_w of 0.010 and 0.011. Tail rotor power is sensitive to the aircraft trim, in particular, the sideslip angle, and this will be examined in the next section.

Trim Effects on UH-60A Performance

The trim results at C_w of 0.0065 (C_w/σ = 0.08) are investigated in detail in Figures 5 through 8. Aircraft attitudes and pilot control angles are shown in Figure 5. The analysis shows fair to good correlation for collective and longitudinal cyclic angles and pitch attitude. However, a large difference is observed in the lateral trim quantities (lateral cyclic angle and roll attitude). Within the data scatter, the flight data were obtained for a zero roll angle, that is, no steady lateral acceleration on the pilot. To accomplish this, the pilot tends to fly with a small amount of sideslip and uses the aircraft's static dihedral to zero the roll angle. The CAMRAD II trim for $\mu > 0.2$ is clearly outside this scatter.

Figure 6 shows blade flap and lag hinge rotation angles. The calculated coning angles are compared with measured values from blades 1 and 2. Steady coning can also be derived from the blade thrust and the centrifugal force (70,883 lb.). The calculated coning angles show good agreement with CAMRAD II estimated values. Thus, it is concluded that there was a bias error in the coning angle measurements. The calculated mean lag angle shows good correlation at $\mu <$ 0.3, considering the scatter of the measured data. At higher speeds, however, the measured data agree well with each other and the analysis shows an overprediction. The calculated longitudinal flapping angles show good correlation up to μ of about 0.2, but overpredict as speed increases. CAMRAD II captures the sudden increase of the longitudinal flapping angle at μ = 0.35. However, the analysis shows a much larger change than the data. The analysis underpredicts lateral flapping angles at all speeds. This is similar to the poor lateral trim predictions shown in Figure 5.

The calculated main rotor shaft pitch and roll moments are compared with flight test data in Figure 7. The trend is the same as the longitudinal and lateral flapping angles.

The calculated tip path plane angles in an inertial coordinate system are compared with measured values in Figure 8 to see the combined effects of a rotor and a fuselage. The tip path plane tilt angles are defined as:

Longitudinal TPP tilt angle = β_{1c} (longitudinal flapping angle) $-$ aircraft pitch attitude $+ 3^\circ$ shaft pre-tilt
Lateral TPP tile angle = β_{1s} (lateral flapping angle) $-$ aircraft roll attitude

The longitudinal tip path plane tilt angles show good correlation at all forward speeds. This result shows that the rotor propulsive force, thus the airframe drag value, is accurate. However, there seems to be an inaccuracy in the lift and pitching moment of the fuselage and stabilator. The calculated lateral tip path plane tilt angles show good correlation up to μ of around 0.2 and then overpredict as speed increases. Although the correlation appears to be better than with roll attitude, there still may be uncertainties other than fuselage aerodynamic characteristics.

To understand the poor to fair correlation of the tail rotor power and lateral trim values, the effect of sideslip was evaluated by looking at changes of $\pm$ 5 degrees. These changes have little influence on the main rotor power and longitudinal TPP tilt angle. As shown in Figure 9, however, a -5 degree sideslip angle trim slightly reduces the tail rotor power at moderate and high speeds, and thus improves the correlation. However, the aircraft roll attitude is increased significantly so that the lateral TPP tilt angle is far from the flight test data. A $+5$ degree sideslip angle trim shows better correlation for the roll attitude and lateral TPP tilt angle but overpredicts the tail rotor power at moderate and high speeds. The lateral flapping angle shows no sensitivity to the sideslip angle change.

The effect of a main rotor to airframe aerodynamic interference on the performance and longitudinal trim values is shown in Figure 10. The main rotor to airframe interference has a small influence on the main rotor and tail rotor power required. The pitch angles are slightly underpredicted at moderate and high speed range without interference. The longitudinal flapping angles, however, show good correlation without interference effects, especially at $\mu > 0.2$.

The effect of a fuselage flat plate area changes on the power coefficient and longitudinal trim values is shown in Figure 11. A 10% change of the flat plate area from the baseline value changes the required power by a maximum of 6.5%. A 10% reduction of the fuselage drag shows good correlation for the longitudinal TPP tilt angle. However, the pitch attitude and longitudinal flapping angle show larger deviations at high speeds.

STD/UH-60L and WCB/UH-60L Performance

The total power coefficient ($\bar{C}_p$) for the STD/UH-60L is calculated and compared with level flight test data in Figure 12. The total power coefficient is the sum of each engine's power and it is normalized to protect Sikorsky's proprietary data. The standard blade was tested on a UH-60L, aircraft 84-23953, as part of the development testing of the wide chord blade. The only difference in modeling between the UH-60A and the STD/UH-60L is the flat plate area of the fuselage. The calculated power coefficient for the STD/UH-60L matches the measured values quite closely. Figure 13 compares the calculated performance of the WCB/UH-60L with flight test data. The normalized power coefficient ($\tilde{C}_p$), which is different from $\bar{C}_p$ used for the STD/UH-60L, is used for this comparison. The analysis shows good correlation up to a weight coefficient $C_w = 0.009$. However, an underprediction is observed at high gross weight and speed. These correlations will be discussed quantitatively in the next section.

CAMRAD II was used to investigate the effects of the new airfoils alone and combined with the increased solidity. Figure 14 shows the angles of attack versus Mach number at C_w = 0.011 and μ = 0.24. These values are calculated from CAMRAD II and plotted at three different spanwise locations (r/R = 0.5, 0.7, and 0.9) and at every 15 degree azimuth angle. At this high gross weight condition, most of baseline blade experiences stall on the retreating side. The addition of the new airfoils to the standard blade has little influence on the angle of attack distribution, and thus stall characteristics. However, the wide chord blade, due to increased solidity, reduces blade loading and thus delays stall inception at this high weight coefficient.

Quantitative Performance Correlation

To characterize the accuracy of the correlation, the performance data have been examined quantitatively. Figures 15 through 17 compare the calculated and measured performance of the UH-60A. Only data for $\mu \geq 0.11$ is included in Figure 15. The 45 deg diagonal line represents a perfect match between analysis and test. The calculated power coefficients lie above the 45 deg line if the analysis overpredicts, and below the line if the analysis underpredicts. The correlation is assessed by fitting a least squares regression line and computing the slope, m. A second measure is the correlation coefficient, r, which provides an indication of dispersion. A third measure is the RMS error from the 45 deg line. A similar approach can be found for the harmonic correlation for oscillatory flap bending moment by Bousman and Maier [8]. CAMRAD II shows good correlation at $\mu \geq 0.11$. Excluding C_w of 0.011 which has few data points, the worst values are: m = 1.060, r = 0.970, and RMS error = 4.6508E-5. Estimated power is underpredicted at low speed ($\mu < 0.11$) except C_w of 0.01, thus both m and

r are significantly less than unity as shown in Figure 16. The main rotor power correlation shows better agreement than the total engine power (Figure 17). Excluding C_w of 0.011, the worst values are: m = 1.045, r = 0.990, and RMS error = 3.4586E-5.

The STD/UH-60L correlation also shows good agreement as in Figure 18. The analysis appears to slightly overpredict at moderate speeds, as was seen with the UH-60A prediction. However, the analysis shows good correlation at moderate speeds in the WCB/UH-60L case as shown in Figure 19.

In general, CAMRAD II underpredicts performance at high gross weight and high speed. Thus, the slope departs from 1, although the correlation coefficient indicates little dispersion. The m, r, and RMS error values for the three aircrafts are tabulated in Table 2 and also shown in Figure 20. The scale of RMS error values of the UH-60L correlation is different from that of the UH-60A correlation due to the normalization of the power coefficients for UH-60L.

The ability of the analysis to predict the performance degrades for all the configurations as the gross weight increases. To understand the performance prediction degradation at high gross weight, the effects of dynamic stall (Leishman-Beddoes model) on the performance were investigated for the wide chord blades. The parameters required for the Leishman-Beddoes model were calculated using CAMRAD II because test values were not available. The calculation with dynamic stall showed minor effects at moderate speed while the power was slightly reduced at high speed.

Conclusions

The analysis CAMRAD II has been used to predict the performance of the UH-60 Black Hawk helicopter with standard and advanced rotors. The analysis has been correlated with the flight test data both qualitatively and quantitatively. From this study the following conclusions are obtained:

UH-60A

1. The predicted total engine power and main rotor power show good agreement with the flight test data at $\mu \geq 0.11$. However, an underprediction is observed at $\mu < 0.11$.

2. The analysis shows fair to good correlation for collective and longitudinal cyclic angles and pitch attitude and poor to fair correlation for the lateral trim quantities (lateral cyclic angle and roll attitude).

3. The tip path plane tilt angles in an inertial coordinate system show that there seems to be an inaccuracy in the fuselage longitudinal aerodynamic characteristics. Although sideslip has a significant influence on the tail rotor power and the aircraft roll attitude, no consistent improvement is obtained.

STD/UH-60L and WCB/UH-60L

1. The analysis shows the same trends as the flight test data. However, an underprediction is observed for the performance of the WCB/UH-60L at high gross weight and speed. The degradation of the ability of the analysis to predict the performance at high gross weight occurs for all the configurations calculated.

2. Increased solidity of the wide chord blade appears to be a dominant factor in the performance improvement at high gross weight by reducing blade loading and thus delaying stall inception.

Acknowledgment

The authors would like to express thanks to Dr. John Berry, Mr. James O'Malley, and Mr. Douglas A. Ehlert at US Army AMCOM and Mr. T. Alan Egolf at Sikorsky Aircraft Corporation for their sharing of valuable data and knowledge.

References

[1] Kufeld, R. M., Balough, D. L., Cross, J. L., Studebaker, K. F., Jennison, C. D., and Bousman, W. G., "Flight Testing of the UH-60A Airloads Aircraft," American Helicopter Society 50th Annual Forum Proceedings, Washington D.C., May 1994.

[2] Bednarczyk, R., Boirun, B., DiPierro, A., Fenaughty, R., Sheets, F., Trainer, T., and West, A., "Growth Rotor Blade Feasibility Demonstration Flight Test Report," SER 702183, May 1996.

[3] Johnson, W., "Rotorcraft Aerodynamics Models for a Comprehensive Analysis," American Helicopter Society 54th Annual Forum Proceedings, Washington, D.C., May 1998.

[4] Kufeld, R. M., and Johnson, W., "The Effects of Control System Stiffness Models on the Dynamic Stall Behavior of a Helicopter," *Journal of the American Helicopter Society*, Vol. 45, No. 4, October 2000.

[5] Mudrick, M., "Main Rotor System Loads," SER 702603, September 1999.

[6] Bernard, R., "YUH-60A/T700 IR Suppressor Full Scale Prototype Test Report," SER 70094, June 1976.

[7] Boirun, B., "Flight Manual Performance Substantiating Report for the UH-60A Helicopter Based on the Multi-Year II Configuration," SER 70279-1, May 1988.

[8] Bousman, W. G., and Maier, T. H., "An Investigation of Helicopter Rotor Blade Flap Vibratory Loads," American Helicopter Society 48th Annual Forum Proceedings, Washington, D.C., June 1992.

[9] "UH-60A External Stores Support System Fixed Provision Fairings Drag Determinations," Final Report, USAAEFA Project No. 82-15-1, May 1984.

[10] "Airworthiness and Flight Characteristics Test of a Sixth Year Production UH-60A," Final Report, USAAEFA Project No. 83-24, June 1985.

[11] "Baseline Performance Verification of the 12th Year Production UH-60A Black Hawk helicopter," Final Report, USAAEFA Project No. 87-32, January 1989.

[12] Shanley, J. P. "Validation of UH-60A CAMRAD/JA Input Model," SER 701716, November 1991.

Table 1 Flat plate area calculation

	Equivalent Flat Plate Drag (sq. ft.)			
	Case 1	Case 2	Case 3	Case 4
Baseline UH-60A	25.69 [7]	26.2 [12]	25.69 [7]	26.2 [12]
ESSS fairing	0.78	0.78	2.5	2.5
wire strike kit	0.21	0.21	1.0	1.0
misc.	0.63	0.63	1.0	1.0
BMH/LASSIE	2.0	2.0	2.0	2.0
test instrumentation	0.83	0.83	0.83	0.83
RDAS	2.81	2.81	2.81	2.81
UH-60A (Airloads program)	32.95	33.46	35.83	36.34

Table 2 Slope, correlation coefficient, and RMS error values

	UH-60A			UH-60A		
C_w	m	r	RMS	m	r	RMS
	($\mu \geq .11$)			($\mu < .11$)		
0.0065	1.015	0.995	2.0225E-5	0.436	0.944	6.2228E-5
0.0074	0.993	0.995	2.8172E-5	0.344	0.916	8.1571E-5
0.0083	1.060	0.994	2.2579E-5	0.907	0.844	7.1231E-5
0.0091	1.052	0.970	4.0415E-5	0.432	0.956	15.240E-5
0.010	1.027	0.992	4.6508E-5	0.459	0.593	6.1474E-5
0.011	0.832	0.867	3.0164E-5	N/A	N/A	N/A

	UH-60A (MR)		
C_w	m	r	RMS
	($\mu \geq .11$)		
0.0065	1.042	0.997	1.4217E-5
0.0074	0.987	0.997	1.2302E-5
0.0083	1.045	0.995	2.9285E-5
0.0091	1.030	0.975	3.4586E-5
0.010	1.018	0.990	1.9127E-5
0.011	0.821	0.908	4.3542E-5

	STD/UH-60L			WCB/UH-60L		
C_w	m	r	RMS	m	r	RMS
0.0065	1.093	0.994	0.021069	1.048	0.996	0.022893
0.0081	1.003	0.988	0.017743	0.987	0.993	0.017304
0.0085	1.034	0.991	0.015666	0.905	0.990	0.017643
0.0091	1.040	0.999	0.057867	0.875	0.995	0.015197
0.010	0.848	0.973	0.026714	0.682	0.990	0.039625
0.011	0.498	0.984	0.053192	0.583	0.966	0.066199

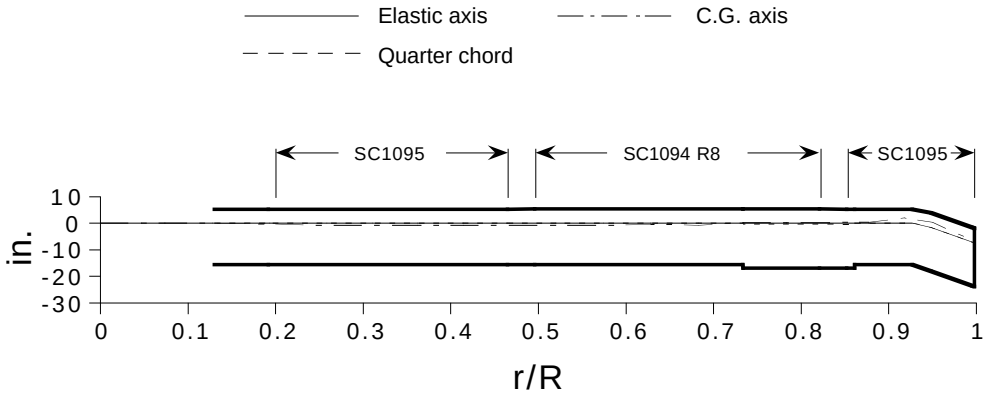

(a) Standard blade

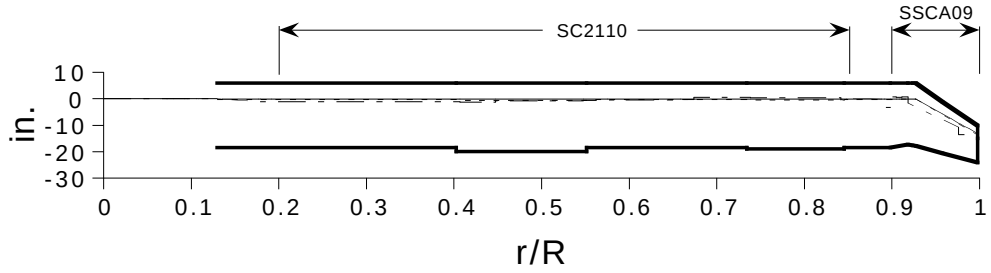

(b) Wide chord blade

Fig. 1 UH-60 Black Hawk rotor blade planform

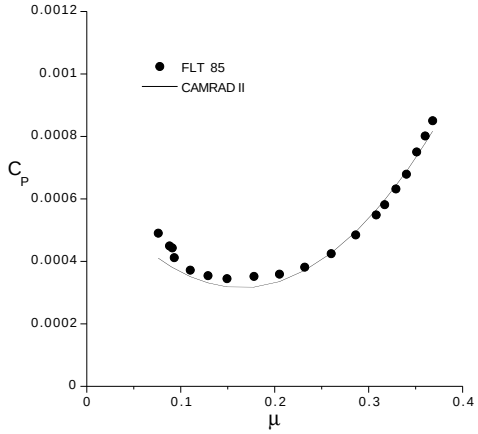

(a) $C_w = 0.0065$

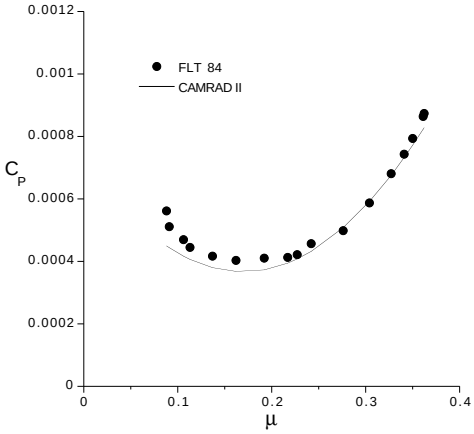

(b) $C_w = 0.0074$

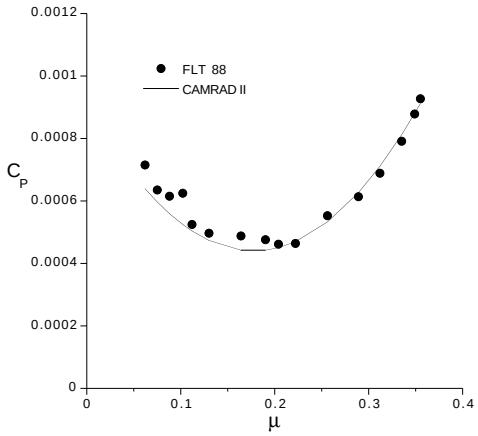

(c) $C_w = 0.0083$

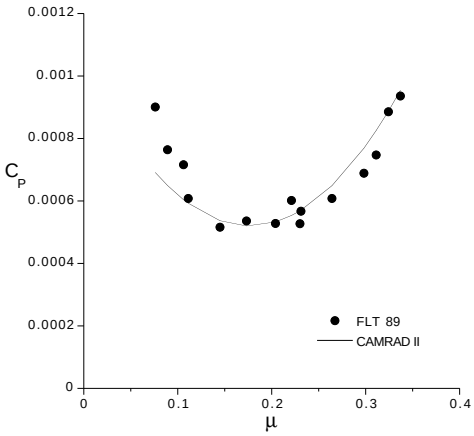

(d) $C_w = 0.0091$

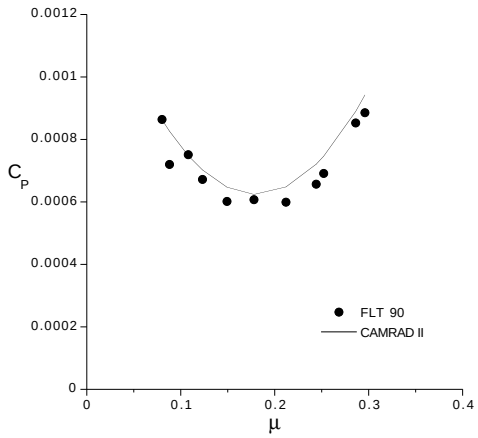

(e) $C_w = 0.010$

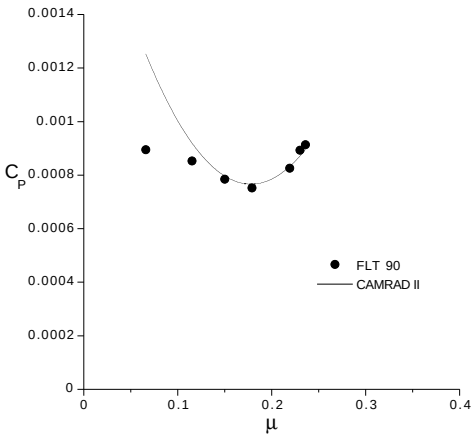

(f) $C_w = 0.011$

Fig. 2 Calculated and measured power coefficient for UH-60A (Airloads Program)

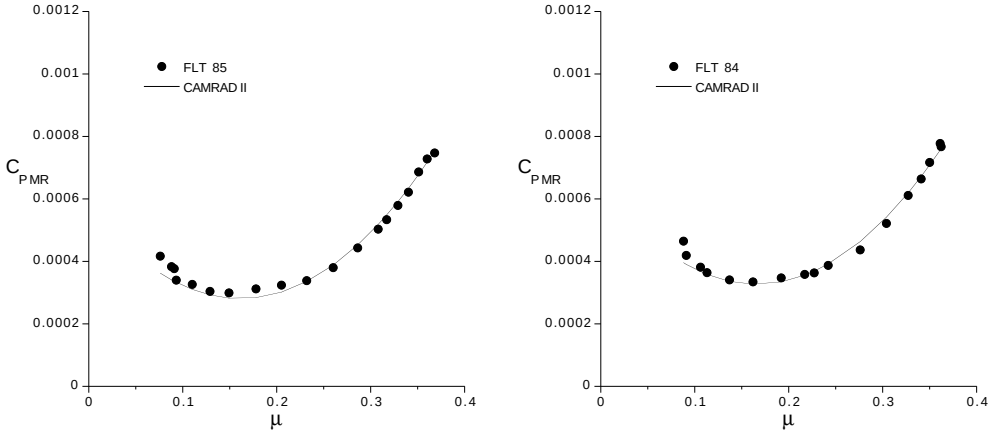

(a) $C_w = 0.0065$

(b) $C_w = 0.0074$

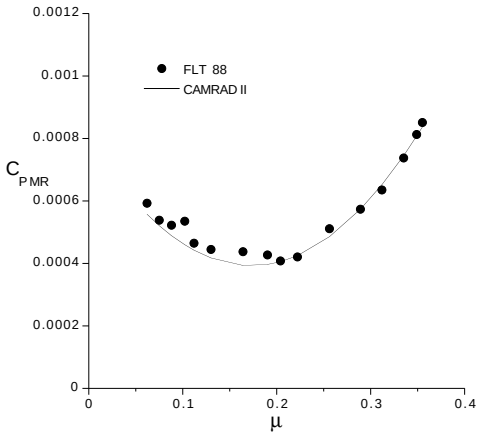

(c) $C_w = 0.0083$

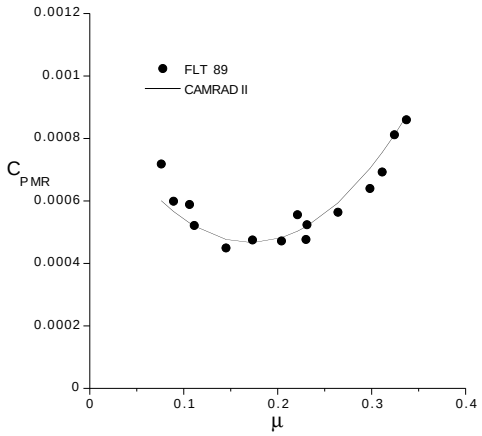

(d) $C_w = 0.0091$

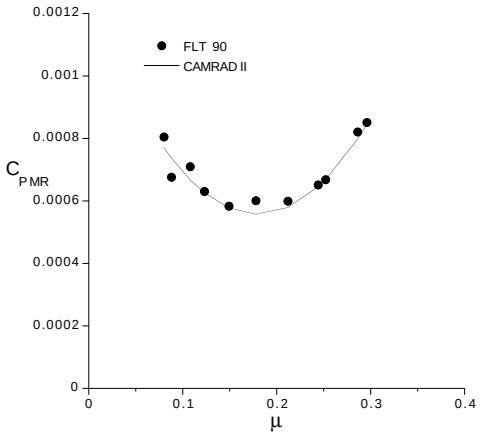

(e) $C_w = 0.010$

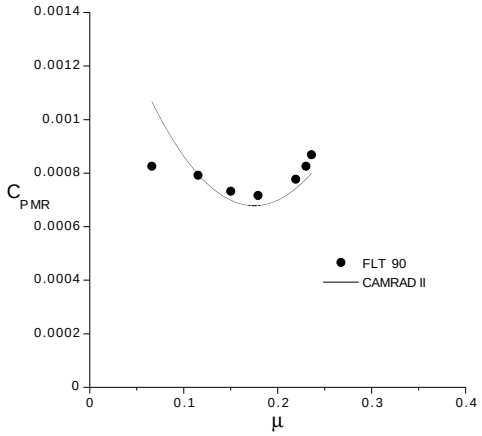

(f) $C_w = 0.011$

Fig. 3 Calculated and measured main rotor power coefficient for UH-60A (Airloads Program)

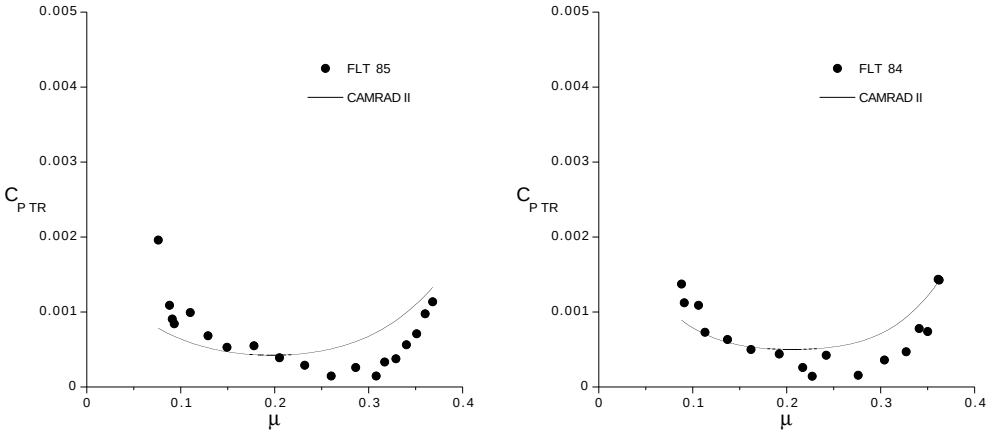

(a) $C_w = 0.0065$

(b) $C_w = 0.0074$

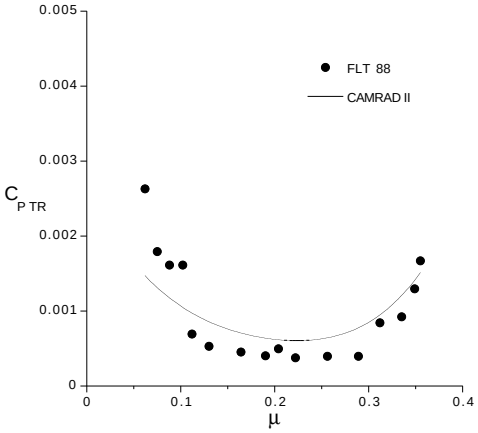

(c) $C_w = 0.0083$

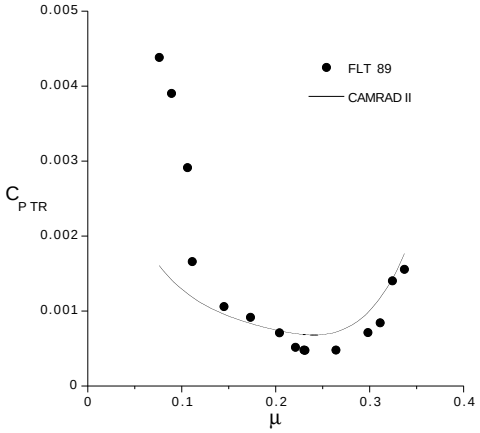

(d) $C_w = 0.0091$

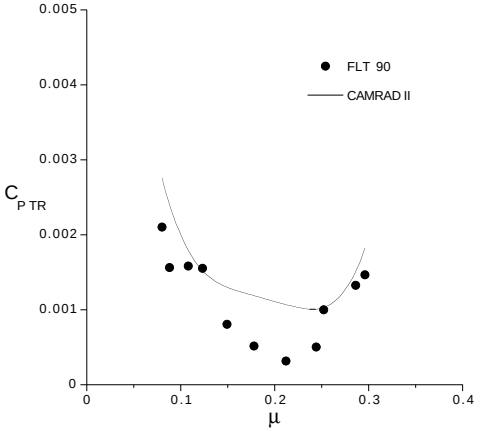

(e) $C_w = 0.010$

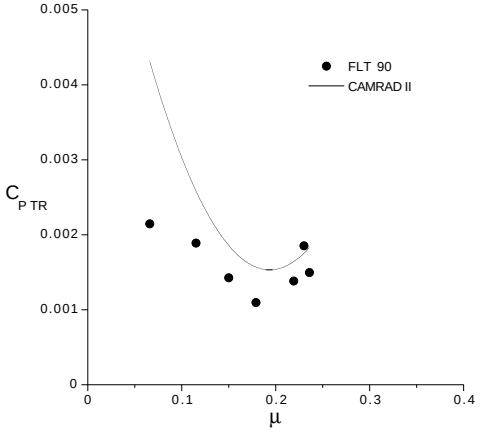

(f) $C_w = 0.011$

Fig. 4 Calculated and measured tail rotor power coefficient for UH-60A (Airloads Program)

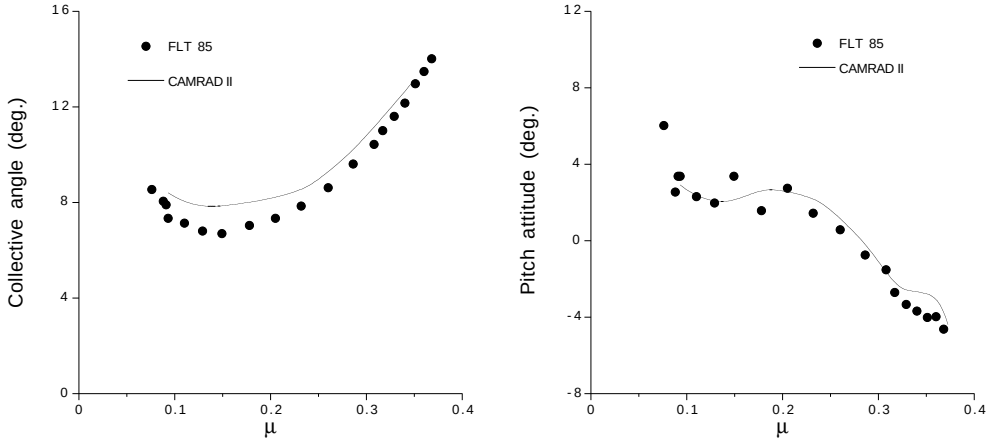

(a) Collective angle

(b) Pitch attitude

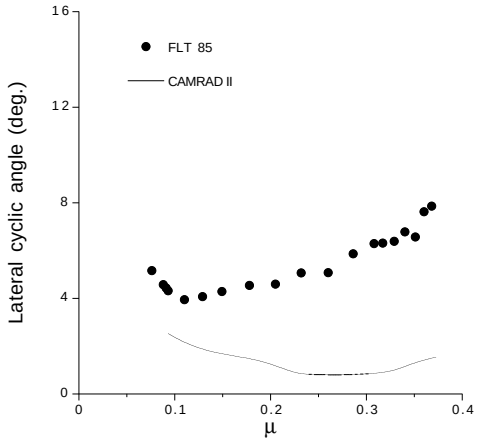

(c) Lateral cyclic angle

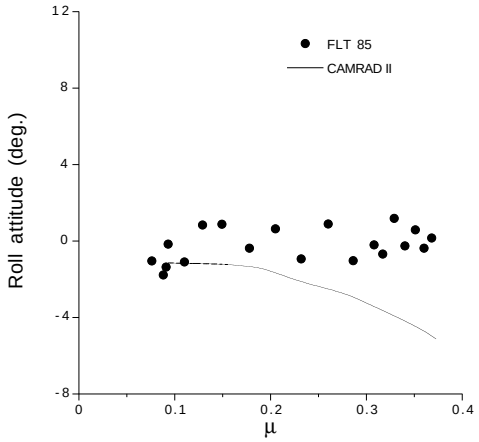

(d) Roll attitude

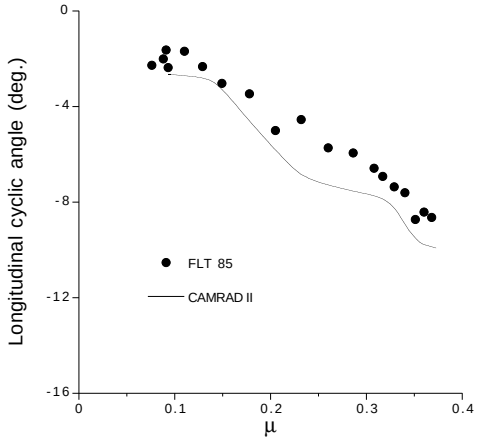

(e) Longitudinal cyclic angle

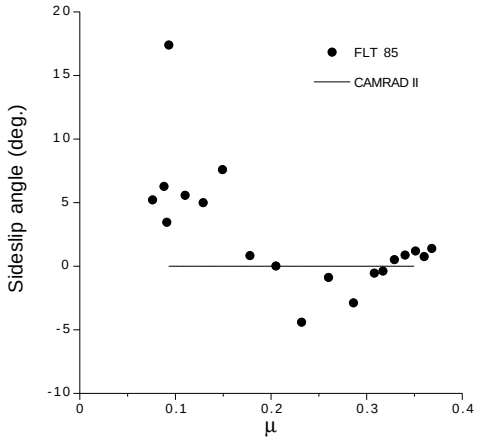

(f) Sideslip angle

Fig. 5 Aircraft attitude and pilot control angles for UH-60A at $C_w = 0.0065$

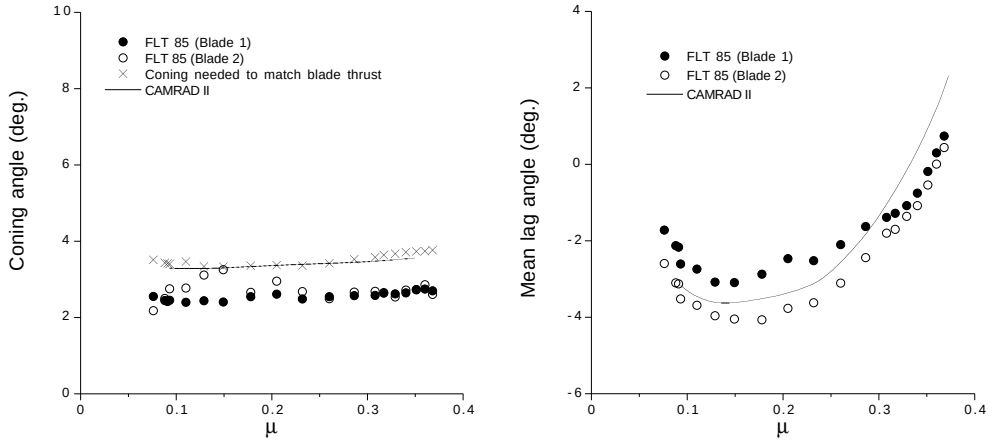

(a) Coning angle

(b) Mean lag angle

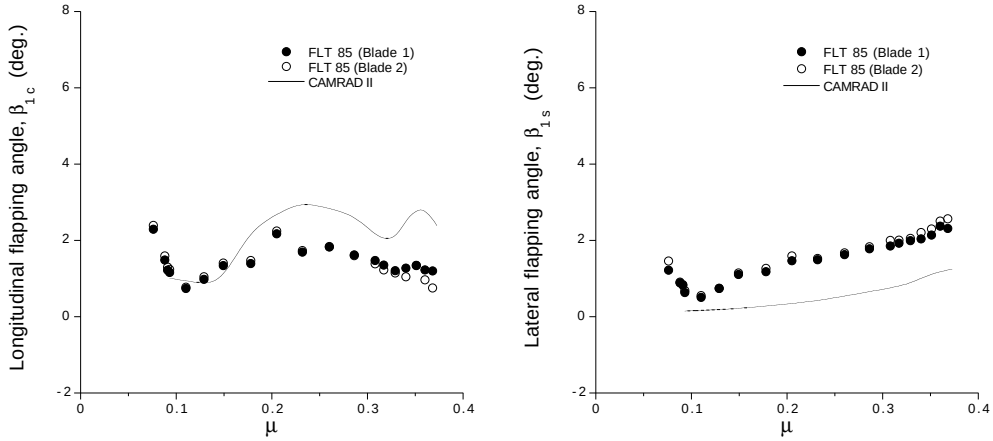

(c) Longitudinal flapping angle

(d) Lateral flapping angle

Fig. 6 Blade flap and lag hinge rotation angle for UH-60A at $C_w = 0.0065$

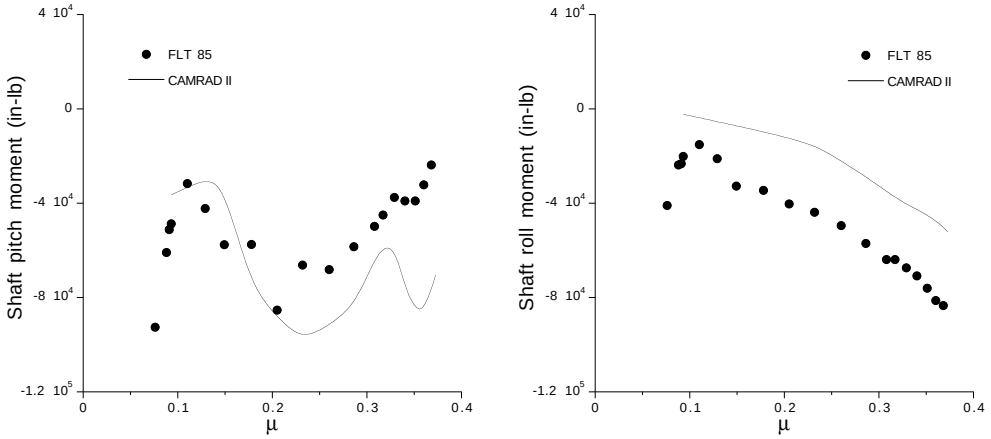

(a) Shaft pitch moment (b) Shaft roll moment

Fig. 7 Main rotor shaft moment for UH-60A at $C_w = 0.0065$

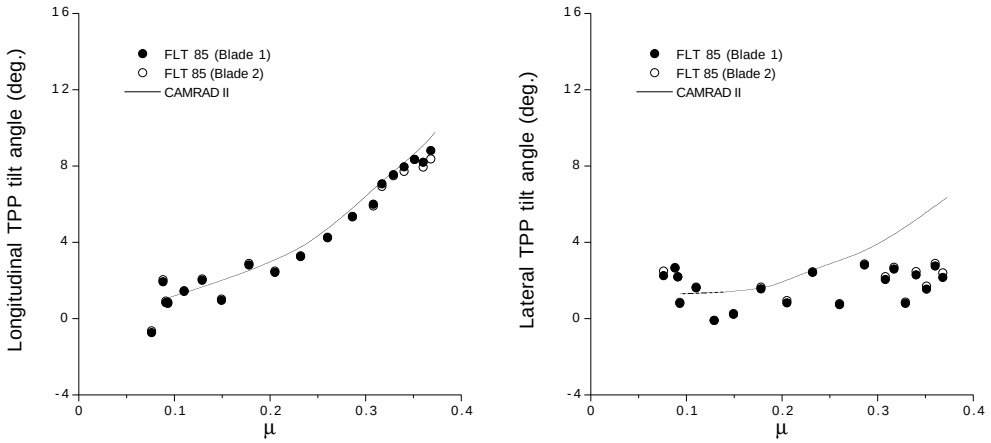

(a) Longitudinal tilt angle (b) Lateral tilt angle

Fig. 8 TPP tilt angle in an inertial coordinate system for UH-60A at $C_w = 0.0065$

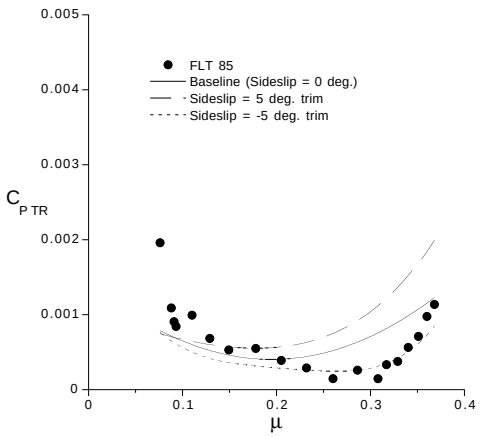

(a) Tail rotor power

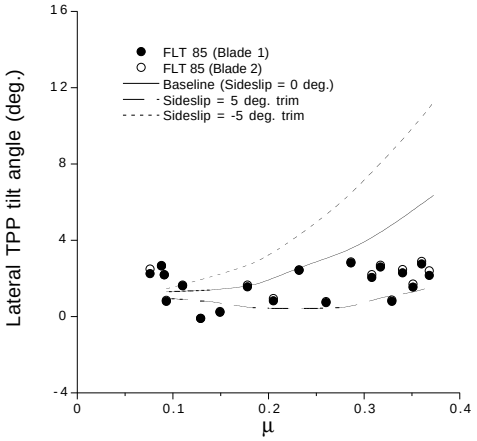

(b) Lateral TPP tilt angle

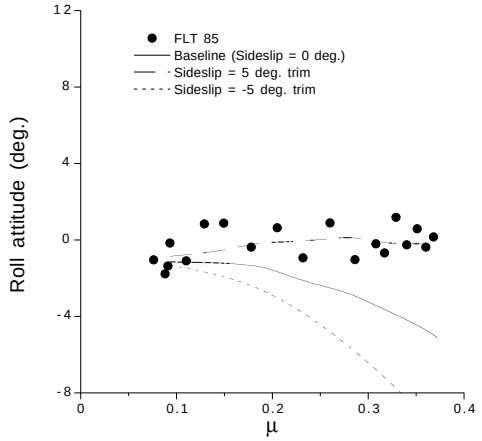

(c) Roll attitude

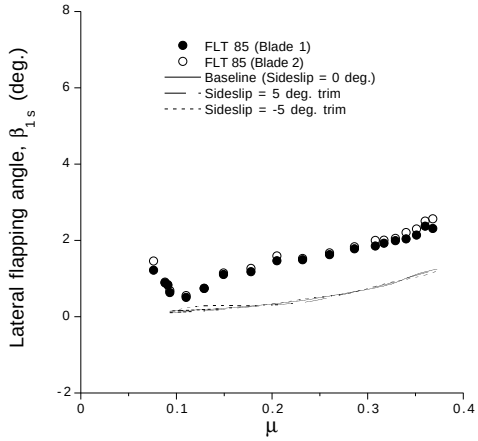

(d) Lateral flapping angle

Fig. 9 Effects of sideslip angle for UH-60A at $C_w = 0.0065$

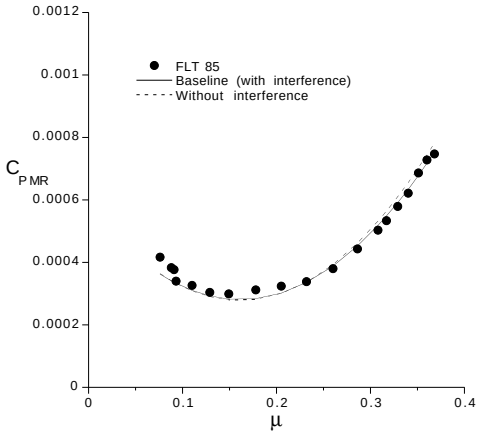

(a) Main rotor power

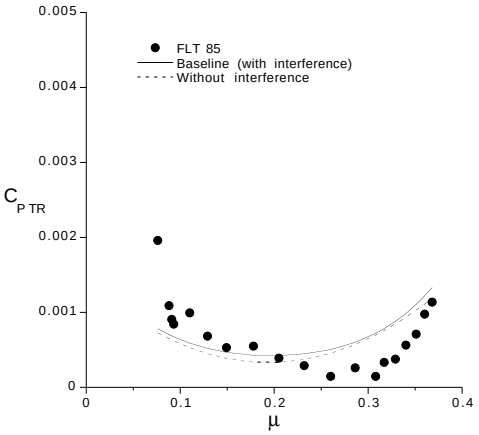

(b) Tail rotor power

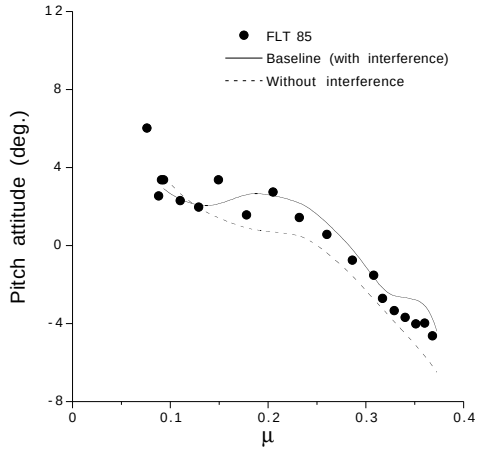

(c) Pitch attitude

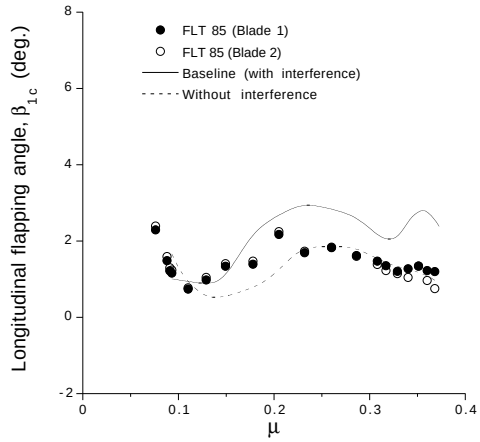

(d) Longitudinal flapping angle

Fig. 10 Effect of interference for UH-60A at $C_w = 0.0065$

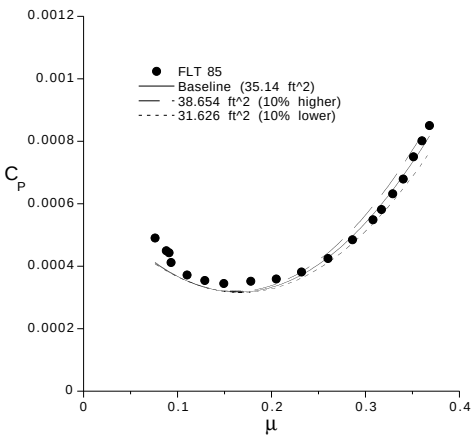

(a) Total power

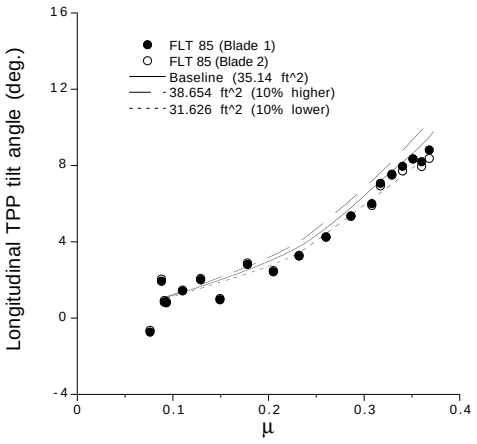

(b) Longitudinal TPP tilt angle

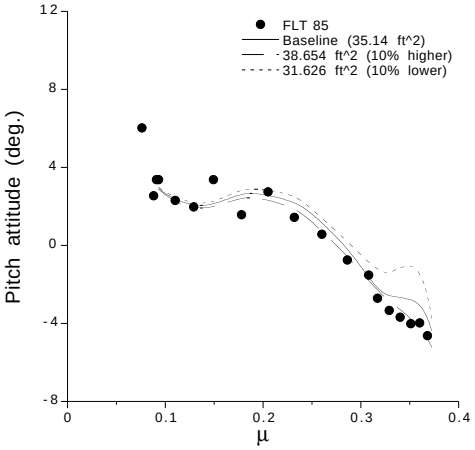

(c) Pitch attitude

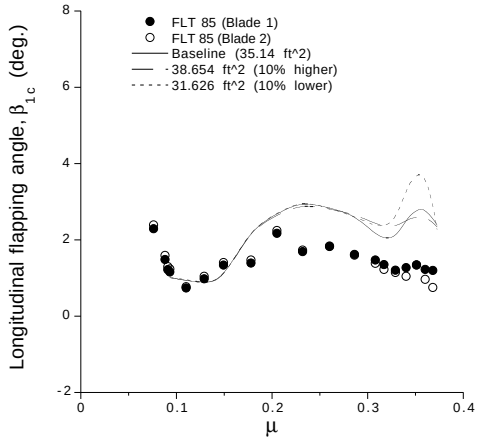

(d) Longitudinal flapping angle

Fig. 11 Effect of fuselage flat plate area for UH-60A at $C_w = 0.0065$

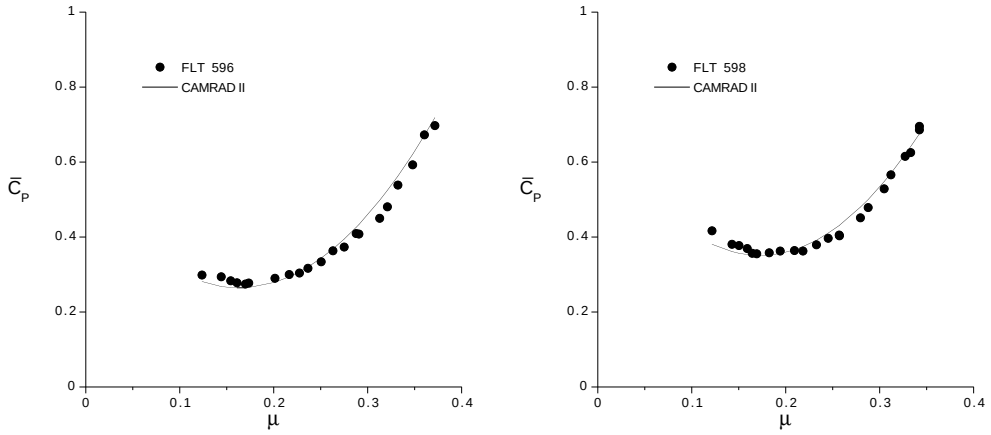

(a) $C_w = 0.0065$

(b) $C_w = 0.0081$

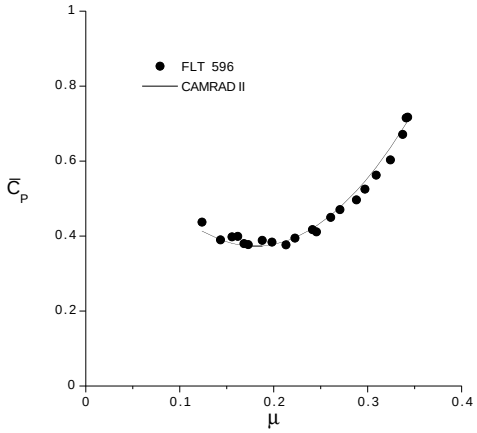

(c) $C_w = 0.0085$

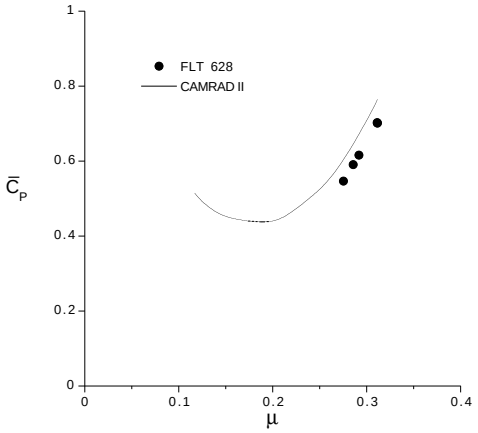

(d) $C_w = 0.0091$

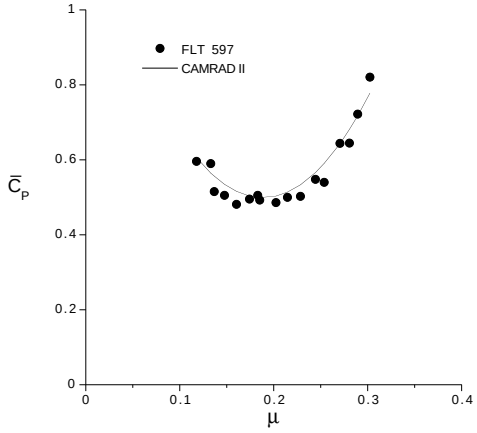

(e) $C_w = 0.010$

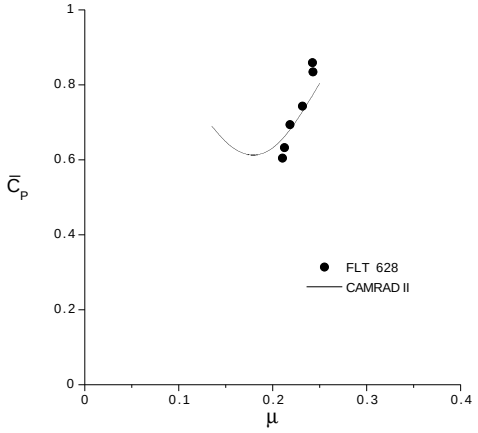

(f) $C_w = 0.011$

Fig. 12 Calculated and measured power coefficient for STD/UH-60L

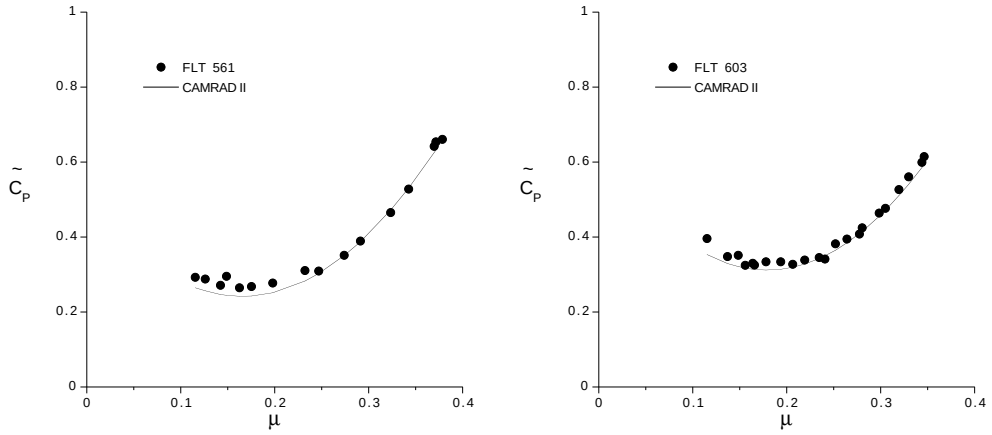

(a) $C_w = 0.0065$

(b) $C_w = 0.0081$

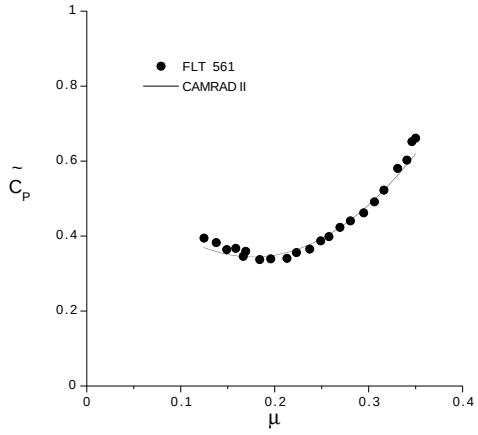

(c) $C_w = 0.0085$

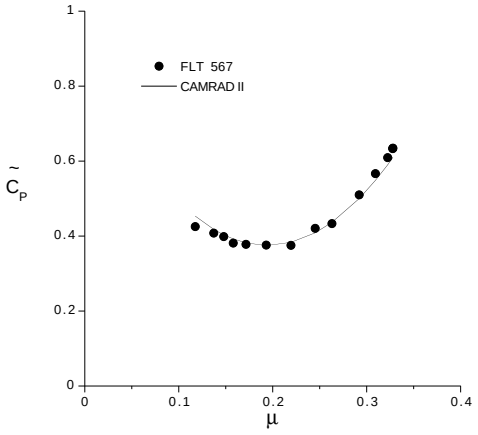

(d) $C_w = 0.0091$

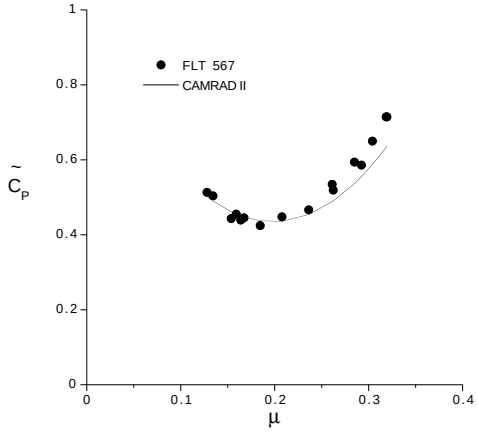

(e) $C_w = 0.010$

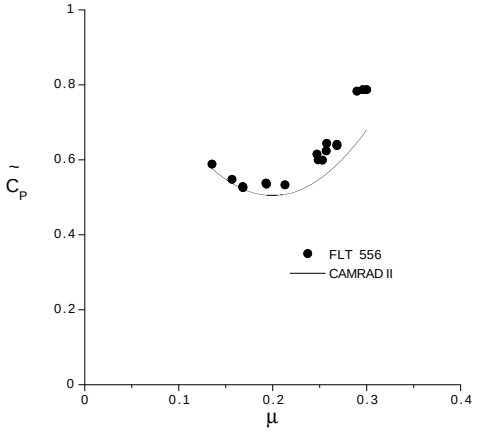

(f) $C_w = 0.011$

Fig. 13 Calculated and measured power coefficient for WCB/UH-60L

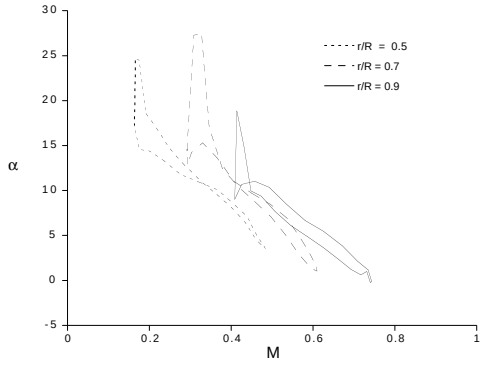

(a) STD/UH-60L

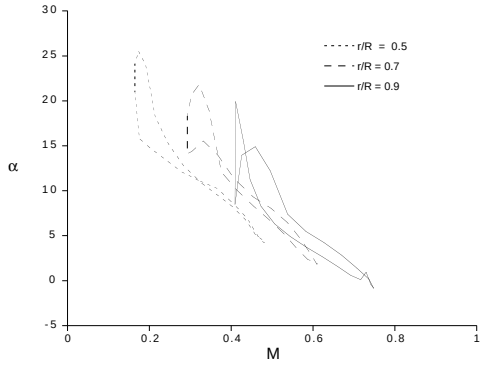

(b) STD/UH-60L with WCB airfoils

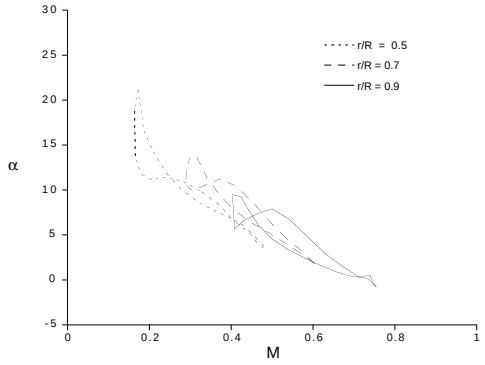

(c) WCB/UH-60L

Fig. 14 Angle of attack versus Mach number at C_w = 0.011 and μ = 0.24

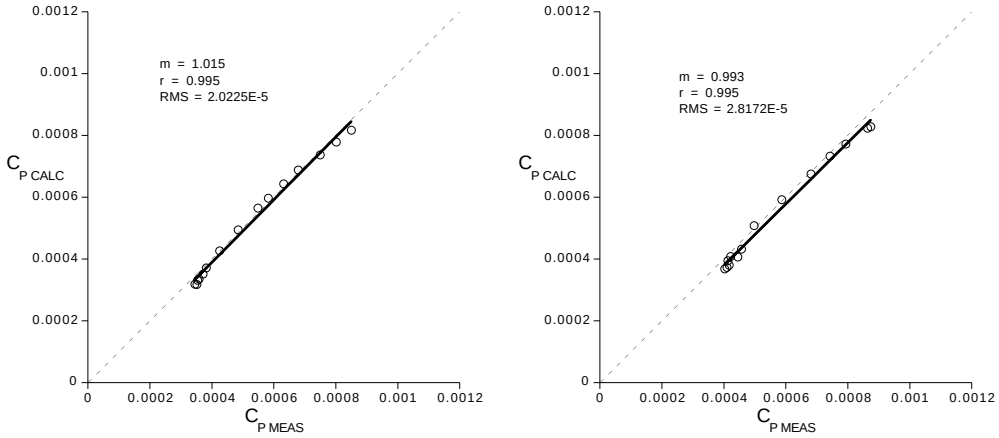

(a) $C_w = 0.0065$ (b) $C_w = 0.0074$

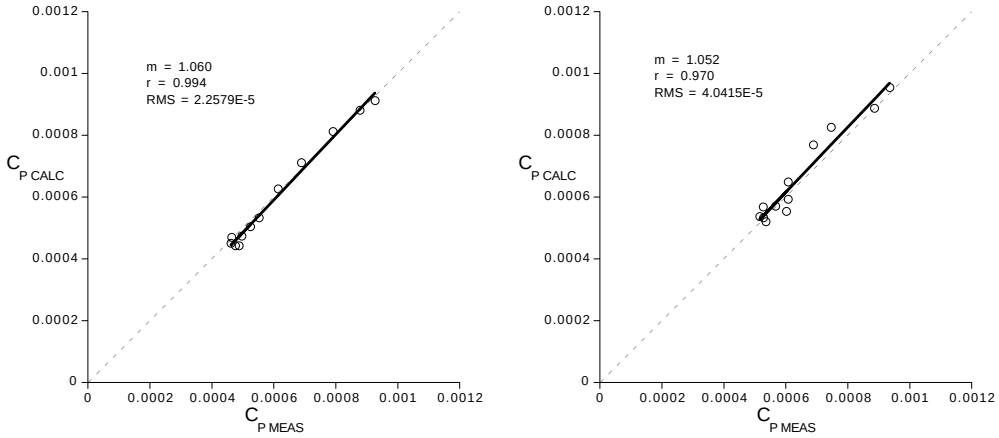

(c) $C_w = 0.0083$ (d) $C_w = 0.0091$

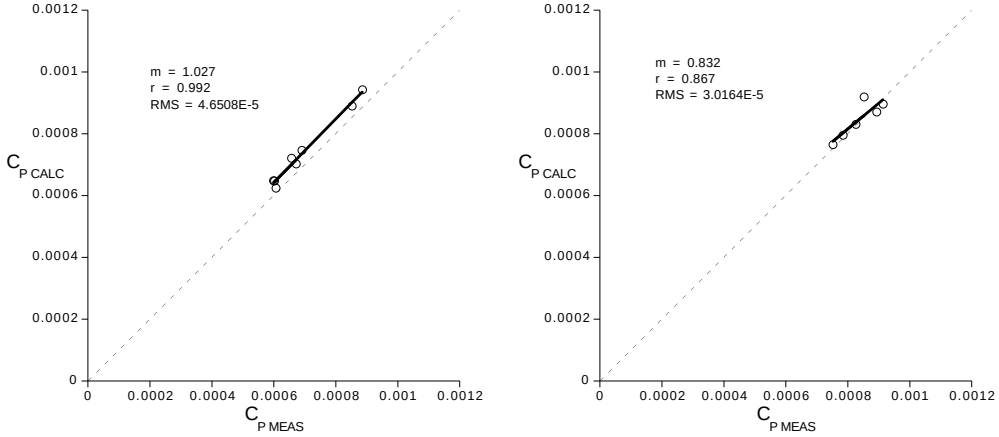

(e) $C_w = 0.010$ (f) $C_w = 0.011$

Fig. 15 Calculated and measured power coefficient for UH-60A (Airloads Program), $\mu \geq .11$

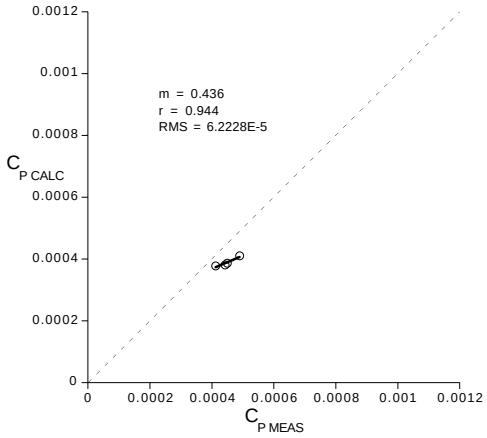

(a) $C_w = 0.0065$

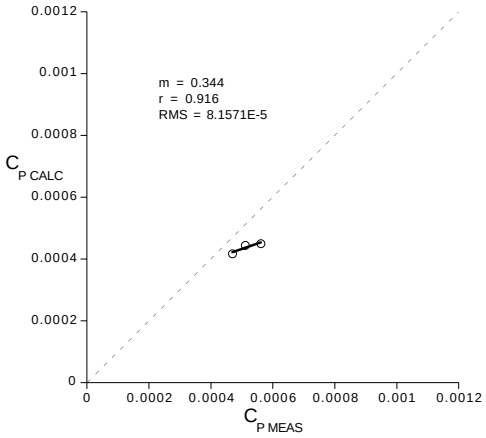

(b) $C_w = 0.0074$

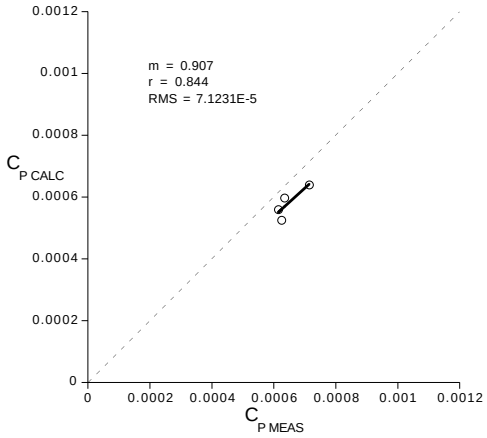

(c) $C_w = 0.0083$

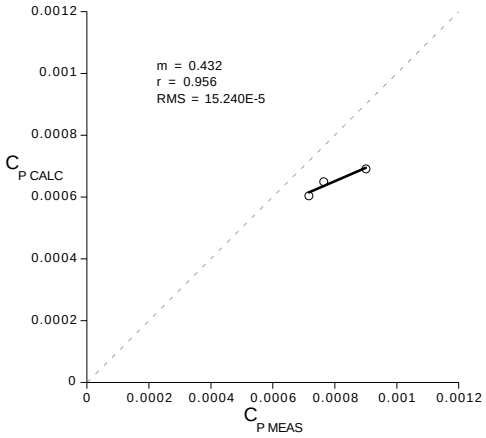

(d) $C_w = 0.0091$

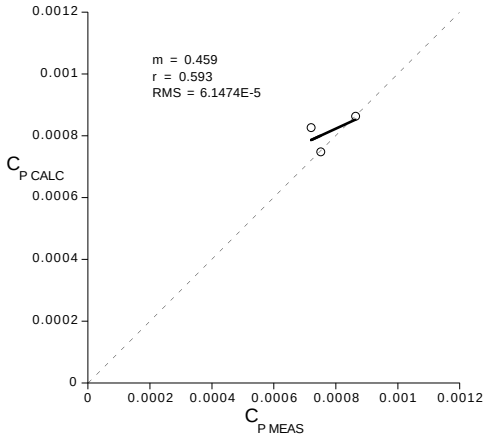

(e) $C_w = 0.010$

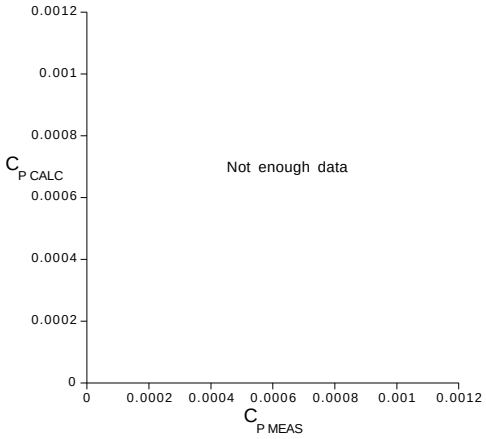

(f) $C_w = 0.011$

Fig. 16 Calculated and measured power coefficient for UH-60A (Airloads Program), $\mu < .11$

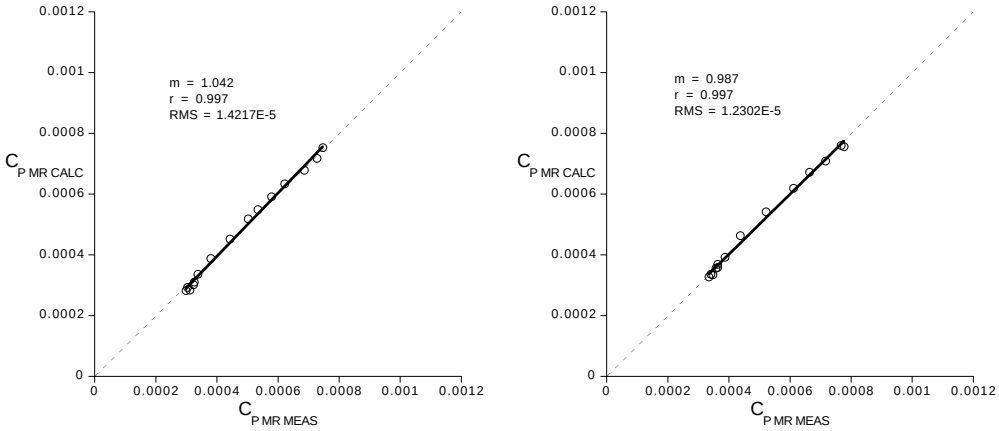

(a) $C_w = 0.0065$ (b) $C_w = 0.0074$

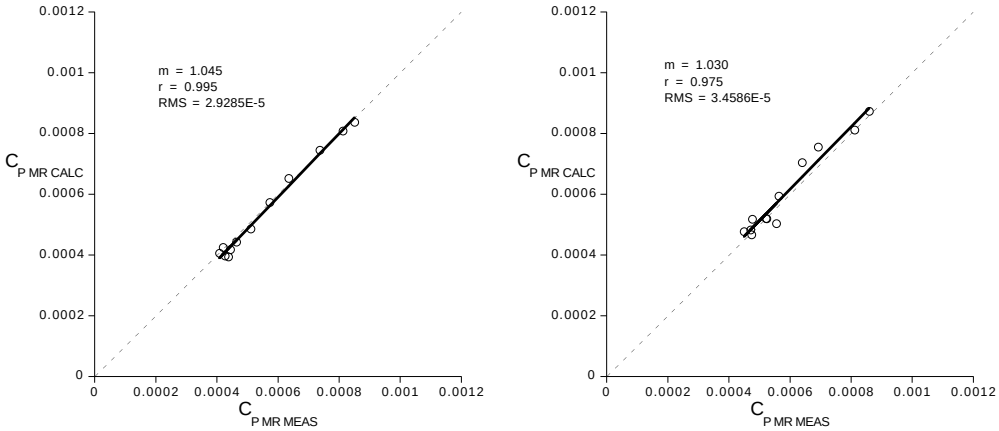

(c) $C_w = 0.0083$ (d) $C_w = 0.0091$

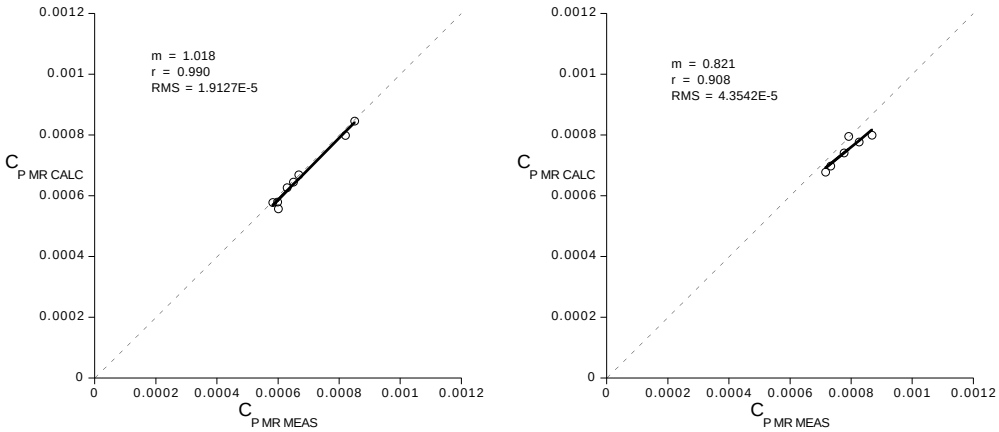

(e) $C_w = 0.010$ (f) $C_w = 0.011$

Fig. 17 Calculated and measured main rotor power coefficient for UH-60A (Airloads Program), $\mu \geq .11$

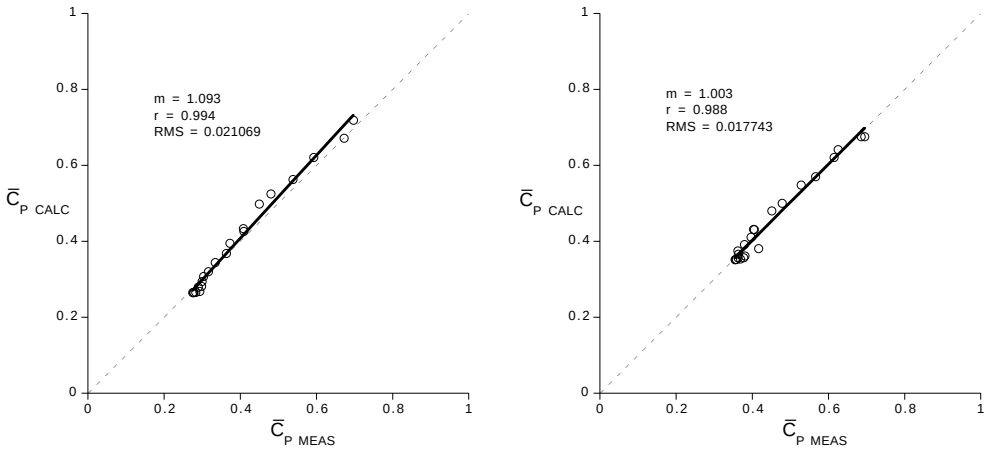

(a) $C_w = 0.0065$

(b) $C_w = 0.0081$

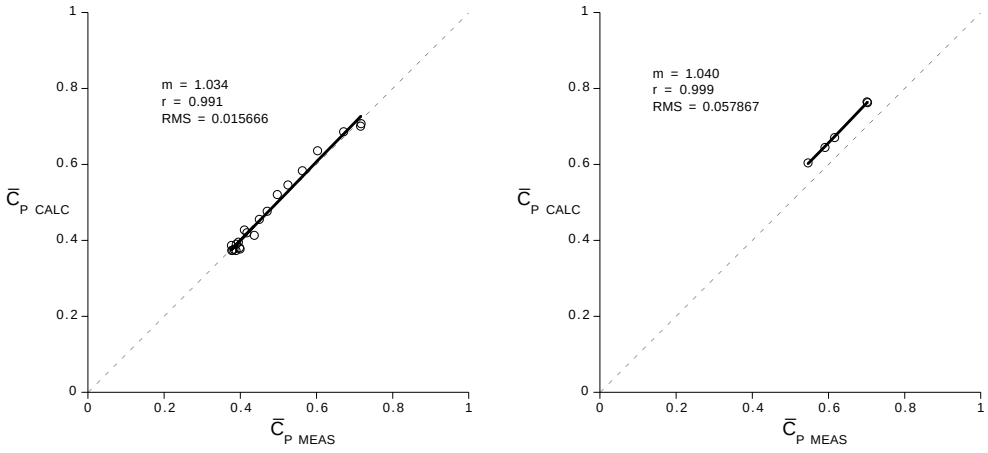

(c) $C_w = 0.0085$

(d) $C_w = 0.0091$

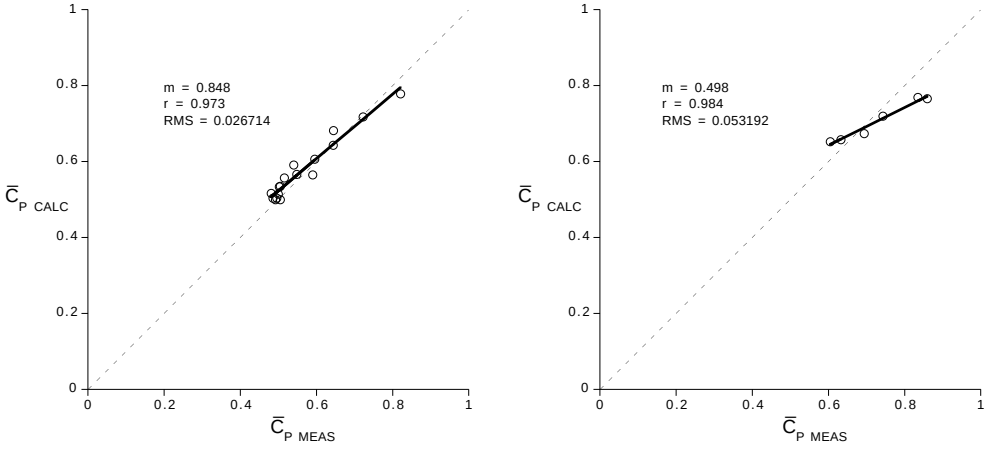

(e) $C_w = 0.010$

(f) $C_w = 0.011$

Fig. 18 Calculated and measured power coefficient for STD/UH-60L

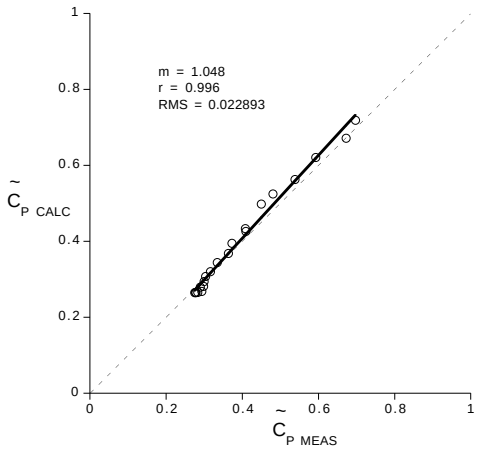

(a) $C_w = 0.0065$

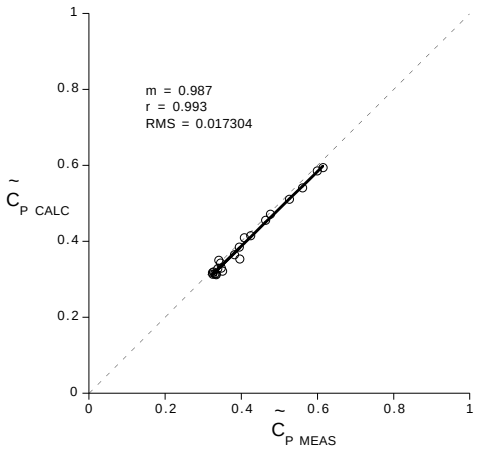

(b) $C_w = 0.0081$

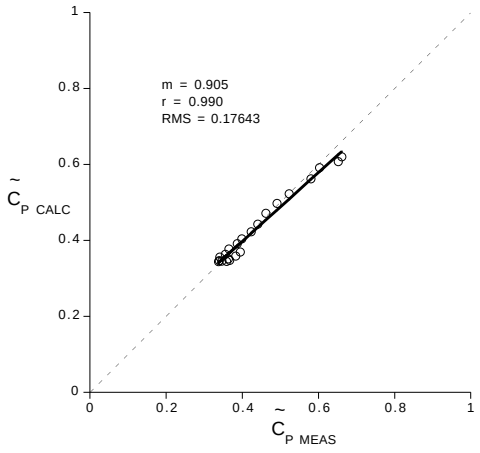

(c) $C_w = 0.0085$

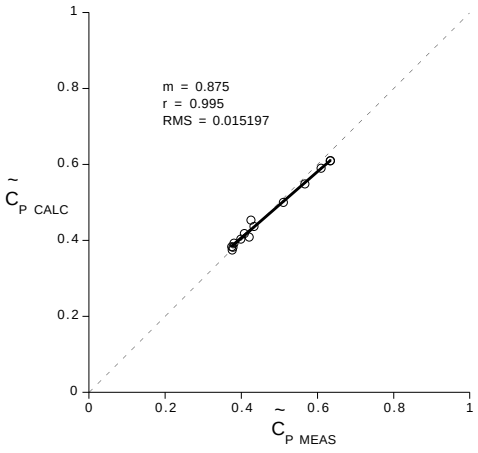

(d) $C_w = 0.0091$

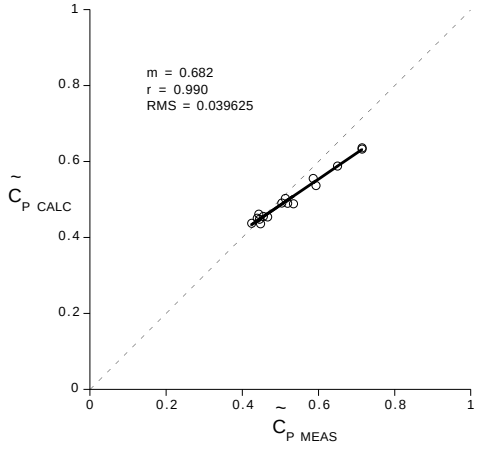

(e) $C_w = 0.010$

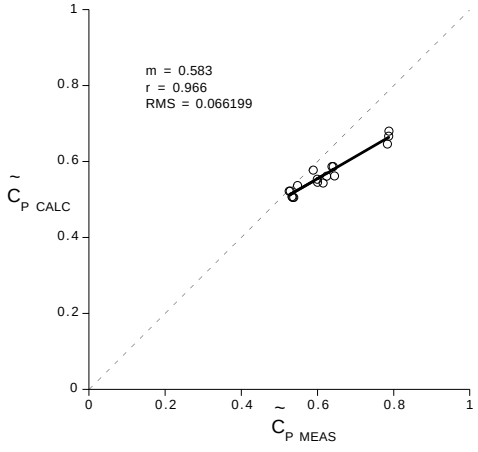

(f) $C_w = 0.011$

Fig. 19 Calculated and measured power coefficient for WCB/UH-60L

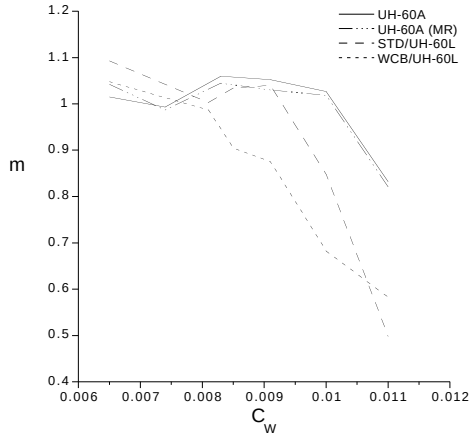

(a) Slope

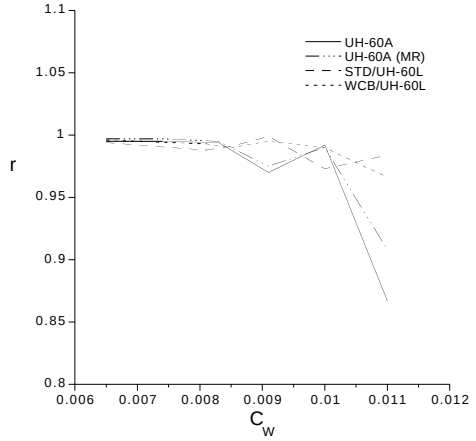

(b) Correlation coefficient

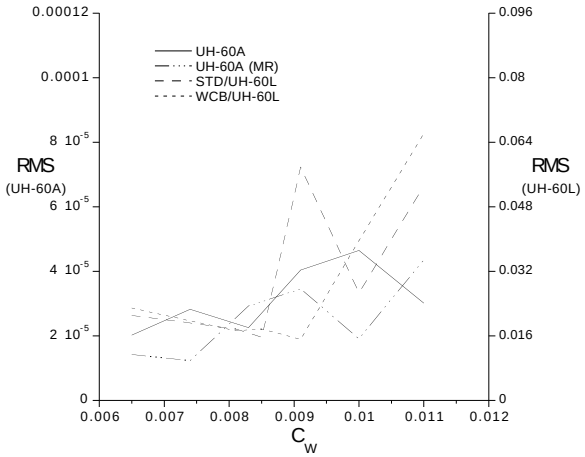

(c) RMS error

Fig. 20 Slope, correlation coefficient, and RMS error values